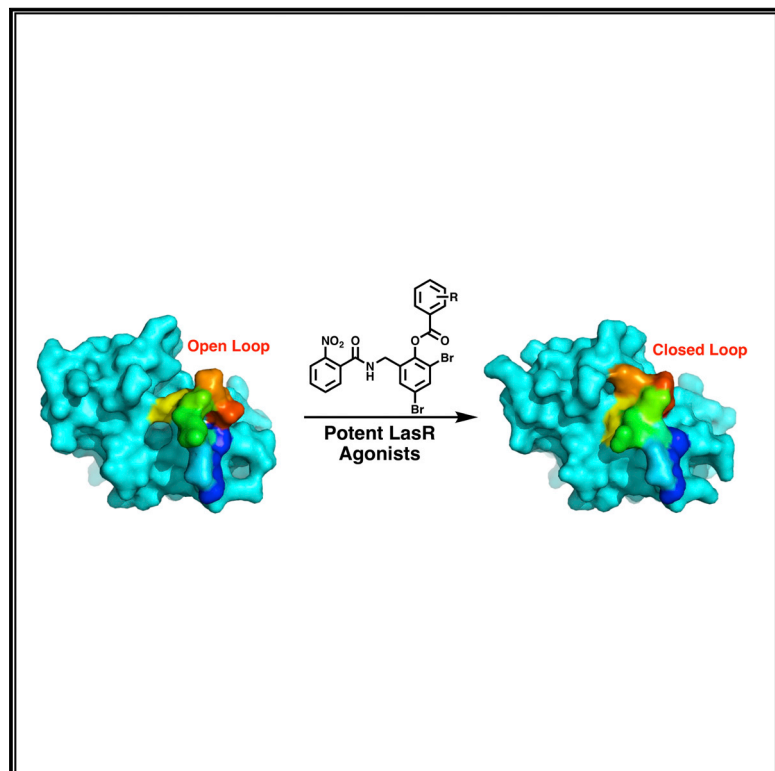


Cell Chemical Biology

Structural and Biochemical Studies of Non-native Agonists of the LasR Quorum-Sensing Receptor Reveal an L3 Loop “Out” Conformation for LasR

Graphical Abstract



Authors

Matthew C. O'Reilly, Shi-Hui Dong, Francis M. Rossi, Kaleigh M. Karlen, Rohan S. Kumar, Satish K. Nair, Helen E. Blackwell

Correspondence

s-nair@life.illinois.edu (S.K.N.), blackwell@chem.wisc.edu (H.E.B.)

In Brief

O'Reilly et al. describe characterization of the LasR quorum-sensing receptor in *P. aeruginosa* with a series of synthetic agonists of different potencies and propose a mechanism by which this LuxR-type receptor recognizes and is activated by synthetic ligands.

Highlights

- A set of triphenyl derivatives was found to activate LasR with varied potencies
- Ligand potency correlated with thermal stabilization of the LasR ligand-binding domain
- Certain agonists altered the conformation of a loop in LasR ligand-binding domain
- A model is proposed for modulation of LasR activity by synthetic ligands

Structural and Biochemical Studies of Non-native Agonists of the LasR Quorum-Sensing Receptor Reveal an L3 Loop “Out” Conformation for LasR

Matthew C. O'Reilly,^{1,3,4} Shi-Hui Dong,^{2,3} Francis M. Rossi,^{1,5} Kaleigh M. Karlen,¹ Rohan S. Kumar,¹ Satish K. Nair,^{2,*} and Helen E. Blackwell^{1,6,*}

¹Department of Chemistry, University of Wisconsin–Madison, 1101 University Avenue, Madison, WI 53706, USA

²Department of Biochemistry, University of Illinois at Urbana–Champaign, 600 S. Mathews Avenue, Urbana, IL 61801, USA

³These authors contributed equally

⁴Present address: Department of Chemistry & Biotechnology, University of Wisconsin–River Falls, River Falls, WI 54022, USA

⁵Present address: Department of Chemistry, SUNY Cortland, Cortland, NY 13045, USA

⁶Lead Contact

*Correspondence: s-nair@life.illinois.edu (S.K.N.), blackwell@chem.wisc.edu (H.E.B.)

<https://doi.org/10.1016/j.chembiol.2018.06.007>

SUMMARY

Chemical strategies to block quorum sensing (QS) could provide a route to attenuate virulence in bacterial pathogens. Considerable research has focused on this approach in *Pseudomonas aeruginosa*, which uses the LuxR-type receptor LasR to regulate much of its QS network. Non-native ligands that antagonize LasR have been developed, yet we have little understanding of the mode by which these compounds interact with LasR and alter its function, as the receptor is unstable in their presence. Herein, we report an approach to circumvent this challenge through the study of a series of synthetic LasR agonists with varying levels of potency. Structural investigations of these ligands with the LasR ligand-binding domain reveal that certain agonists can enforce a conformation that deviates from that observed for other, often more potent agonists. These results, when combined with cell-based and biophysical analyses, suggest a functional model for LasR that could guide future ligand design.

INTRODUCTION

Many common bacteria use an intercellular signaling mechanism called quorum sensing (QS) to coordinate collective behaviors at high cell number (Rutherford and Bassler, 2012; Whiteley et al., 2017). These group behaviors are often related to virulence, as is the case for the Gram-negative opportunistic pathogen, *Pseudomonas aeruginosa* (Lyczak et al., 2000), allowing the bacteria to amass a sufficient population density before effectively attacking a host. In basic terms, QS is regulated by (1) the production of small-molecule or peptide signals — the concentration of which increases with cell number — and (2) the binding of these signals to cognate receptors. Consequently, attenuation of QS signaling using non-native small molecules

or macromolecules has been proposed as an anti-virulence strategy to mitigate bacterial pathogenicity, and concomitantly engender resistance at a potentially slower rate than traditional antibiotics that target bacterial viability (Gerdt and Blackwell, 2014; Mellbye and Schuster, 2011). Toward this end, chemical modulators have been developed for a variety of QS receptors (Galloway et al., 2011), including LasR, a principal regulator of *P. aeruginosa* QS in various environmental contexts (Welsh and Blackwell, 2016a, 2016b).

Gram-negative bacteria typically use *N*-acylated L-homoserine lactone (AHL) signals for QS, which can diffuse or are actively effluxed out of the cell and into the local environment (Papenfort and Bassler, 2016; Schuster et al., 2013; Whiteley et al., 2017). Signal concentration increases with population density, and once the AHL signal concentration reaches a threshold level within the cell, these signals will productively bind their cognate intracellular receptors, the LuxR-type family of transcriptional regulators. The activated LuxR-type receptors then alter gene expression levels to initiate behaviors that will benefit the group and/or are only achievable as a bacterial community, including a range of phenotypes such as biofilm formation, protease and toxin production, and motility mechanisms (Lyczak et al., 2000). The pathogen *P. aeruginosa* has a fairly complex QS circuit involving three LuxR-type receptors (LasR, RhlR, and QscR) (Asfahl and Schuster, 2018), two AHL signals (*N*-(3-oxo)-dodecanoyl HL, OdDHL [compound **1** in Figure 1A] and *N*-butanoyl HL, BHL) produced by LuxI-type synthases (LasI and RhlI, respectively), and the *Pseudomonas* quinolone signal (PQS), which binds to PqsR, a transcription factor unrelated to LuxR-type receptors (Welsh and Blackwell, 2016a, 2016b). It has been proposed that targeting LasR may have the largest impact on QS-related virulence in *P. aeruginosa* (Galloway et al., 2012), since LasR activation directly upregulates certain virulence phenotypes (e.g., proteases, biofilm) and indirectly upregulates other virulence phenotypes (e.g., pyocyanin, rhamnolipid) through positive regulation of both the RhlR and PqsR systems (Asfahl and Schuster, 2018; Welsh and Blackwell, 2016a, 2016b). Therefore, considerable efforts have been directed toward designing molecules to antagonize LasR and thereby block its associated virulence

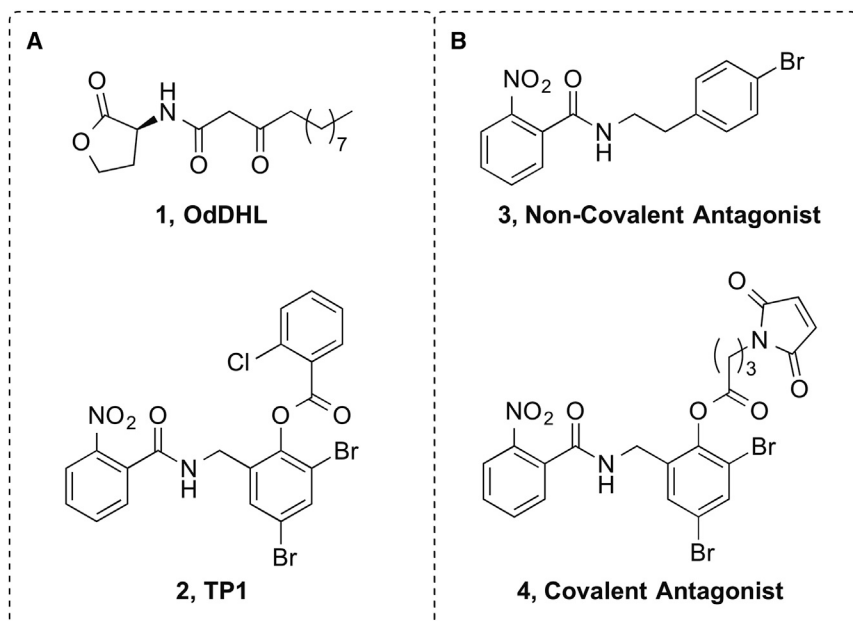


Figure 1. Chemical Structures of Native and Non-Native LasR Ligands

(A) Structures of potent LasR agonists OdDHL (1) and TP1 (2).

(B) Structures of TP-derived antagonists of LasR (3 and 4).

LasR antagonists (Amara et al., 2009; Galloway et al., 2011; Geske et al., 2007), various laboratories have sought to develop TP-derived compounds that antagonize LasR (Figure 1B) (Capitato et al., 2017; O'Brien et al., 2015; O'Reilly and Blackwell, 2016). The antagonists identified in these past studies are among the most potent LasR antagonists known; however, they are orders of magnitude less potent than LasR's native ligand or TP1 (i.e., micromolar half-maximal inhibitory concentration [IC₅₀] values relative to nanomolar half-maximal effective concentration [EC₅₀] values for OdDHL and TP1).

phenotypes, with notable contributions from the Bassler (O'Loughlin et al., 2013), Blackwell (Gerdt et al., 2014; Geske et al., 2007; Moore et al., 2015; O'Reilly and Blackwell, 2016), Greenberg (Müh et al., 2006a, 2006b), Meijler (Amara et al., 2009, 2011), Spring (Galloway et al., 2011; Hodgkinson et al., 2012), and Suga (Smith et al., 2003a, 2003b) laboratories.

Similar to other LuxR-type proteins, LasR is composed of two independently folded domains: a larger amino-terminal ligand-binding domain (LBD) and a smaller C-terminal DNA-binding domain (DBD) (Bottomley et al., 2007; Zou and Nair, 2009). Binding of its native AHL, OdDHL (1), presumably stabilizes monomeric LasR and promotes dimerization of two LasR subunits. The resulting ligand-bound homodimer is then capable of binding DNA and activating transcriptional changes. Such an associative mechanism is predicted for the majority of the known LuxR-type receptors (Churchill and Chen, 2011; Papenfort and Bassler, 2016). While a structure of full-length LasR is yet to be reported, the structure of the LasR-LBD has been solved in complex with various agonists, including LasR's native ligand, OdDHL (1), and three triphenyl (TP)-type compounds that are known to strongly activate the receptor, including TP1 (2) (Figure 1A) (Bottomley et al., 2007; Zou and Nair, 2009). These structural data establish LasR's LBD as an α - β - α sandwich that fully encapsulates these two structurally dissimilar ligand classes (i.e., AHL and TP).

In comparing the previously reported LasR-LBD structures (Bottomley et al., 2007; Zou and Nair, 2009), the LBD is essentially identical when bound to either ligand class, with a main chain root-mean-square deviation (RMSD) of 0.52–0.69 Å. The TP ligands, originally reported by Müh et al. (2006a, 2006b), are of particular interest as LasR modulators, as they are highly potent LasR agonists (comparable with the native ligand OdDHL, 1) and provide a structural scaffold that is more amenable to synthetic diversification relative to AHL-type ligands (Moore et al., 2015; O'Reilly and Blackwell, 2016). By scrutinizing the LasR-LBD structural data in concert with prior activity data for AHL-derived

This low potency has limited the utility of TP-type compounds as chemical tools, as it is difficult for these compounds to outcompete the native QS signal (OdDHL, 1) produced by *P. aeruginosa*. This activity profile is not limited to TP-type LasR antagonists but is also observed for AHL-type LasR antagonists and antagonists of other LuxR-type receptors (Galloway et al., 2012; Welsh and Blackwell, 2016b).

The origins of these low potencies for LuxR-type receptor antagonists are likely multifold. However, we currently have a very limited understanding of the mechanisms by which synthetic ligands antagonize LuxR-type protein activity. With the notable exception of CviR (Chen et al., 2011), studies focused on QS antagonism have been thwarted by the low intrinsic stability of most LuxR-type proteins in the absence of an agonist-type, and thus structure-stabilizing, ligand. Indeed, beyond one recent report (Suneby et al., 2017), the instability of LasR has largely precluded *in vitro* studies with synthetic antagonists. Further characterization of LasR's interactions with synthetic ligands would most certainly facilitate the informed design of chemical agents that modulate LasR, as either antagonist or agonists, with enhanced potencies. We sought to further elucidate these interactions in the current study using a chemical and structural biology approach.

As the LasR-LBD is known to be amenable to structural analysis in the presence of agonists (Bottomley et al., 2007; Zou and Nair, 2009), we reasoned that we could leverage this attribute and gain insights into LasR:ligand interactions by characterizing structures of LasR with a suite of TP-derived agonists with varying degrees of potency (i.e., low to moderate to high). Further, as the structure-activity relationships (SAR) of the promising TP scaffold are still to be fully delineated, we wanted to simultaneously evaluate the SAR of this chemotype and assess whether TP analogs of varied potency could provoke structural changes in LasR, which could also provide insights into the dynamics of receptor:ligand binding and activation.

Herein, we report our design and evaluation of a set of TP analogs displaying variable degrees of LasR agonism in both

cell-based and *in vitro* assays, and our characterization of their interactions with the LasR-LBD using calorimetric and structural biological methods. The structural data for the LasR-LBD complexed to certain agonists reveal deviations when compared with the LasR-LBD complexed to other, often stronger agonists in a loop from Leu-40 to Phe-51, previously termed the L3 loop (Zou and Nair, 2009). We used these data to develop a model by which LasR's L3 loop may govern receptor stability, ligand exchangeability, and signal transduction from the LBD to LasR's DBD. This model provides a different vantage point from which to design LasR modulators, capable of either directly or indirectly interacting with the L3 loop.

RESULTS

A Synthetic Route toward TP1 that Facilitates Analog Synthesis

To expedite the synthesis of TP derivatives with varying potencies, we noted that clear retrosynthetic disconnections exist at the amide and ester bond linkages of TP1 (2). Therefore, we began our synthesis with commercially available hydroxybenzocnitrile 5 (Scheme 1). After screening a variety of reducing agents, conditions employing catalytic nickel boride to reduce the nitrile with concomitant Boc protection of the resulting amine were chosen (Caddick et al., 2003). While the yield of this reduction was moderate, it provided 6 with both heteroatoms in place for ester and amide bond formation in a single step from inexpensive starting materials. Acylation of the resulting phenol with 2-nitrobenzoyl chloride provided ester 7 in high yield. Trifluoroacetic acid was then utilized for Boc cleavage, which resulted in spontaneous ester to amide group transfer fashioning amide 9. Crude 9 was then treated with 2-chlorobenzoyl chloride, providing TP1 in 94% yield over two steps. This 4-step reaction sequence is the most expedient and highest yielding route to TP1 reported to date and enabled straightforward analog synthesis (Zakhari et al., 2011).

Substitution of the Aryl Rings Only Modestly Affects TP Ligand Potency

Using our optimized synthetic route, we prepared a focused library of 14 TP1 (2) analogs, mainly examining the sterics and electronics of the terminal aryl rings of TP1 (structures listed in Table 1). Our primary screen for compound activity utilized an *Escherichia coli* strain harboring a LasR expression plasmid that reports LasR activity via β -galactosidase production through a promoter fusion (see Supplemental Information) (Chugani et al., 2001; Griffith et al., 2002; Lee et al., 2006; Lindsay and Ahmer, 2005). For context, OdDHL (1) and TP1 (2) were screened for LasR agonism in this assay, and produced EC₅₀ values of 1.78 and 0.92 nM, respectively. We began by testing analogs with various electron-withdrawing or -donating substituents on the ester aryl ring (compounds 10–16). Despite the varying properties of these substituents, all of these TP1 analogs still strongly agonized LasR (efficacies \geq 91%), with EC₅₀ values ranging from 0.67 to 9.20 nM (Table 1). We next examined analogs with 2-chloro substituents replacing the nitro group of TP1 (22 and 23). This modification also had only modest impacts on ligand activity, as the compounds remained full LasR agonists with about 5- or 8-fold increases in EC₅₀ (i.e., losses in potency)

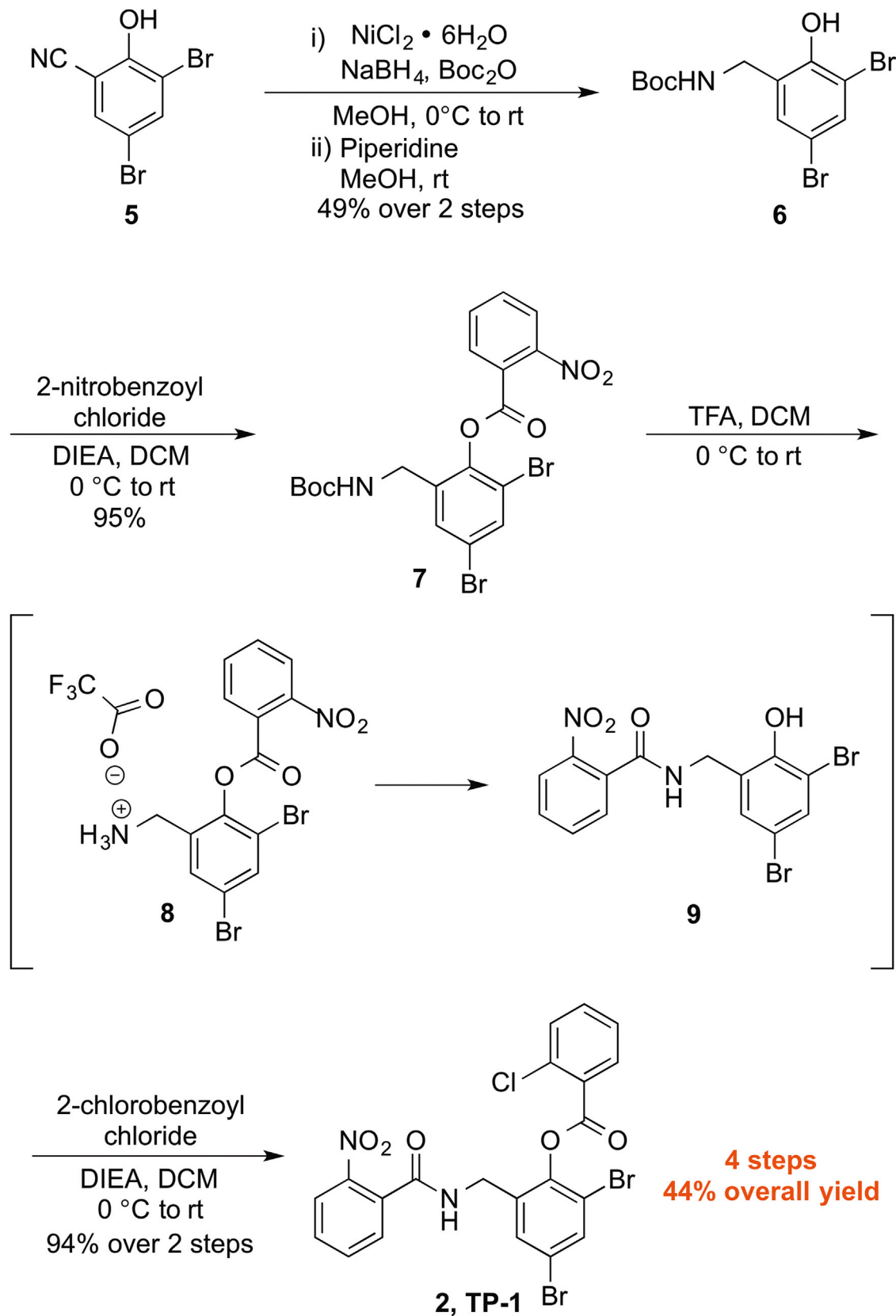
compared with TP1. These results indicated that more substantial changes to the TP1 ligand scaffold would be required to obtain LasR agonists with larger potency differences.

Truncated TP Analogs Display Reduced Potencies yet Maintain Full LasR Agonism

As the co-crystal structure of LasR-LBD:TP1 indicates that the TP1 ester aryl ring makes a large number of hydrophobic contacts in the LBD (Zou and Nair, 2009), we expected a hydrophobic group in this region would be necessary to provide full agonism of LasR. We began to probe the importance of the hydrophobic contacts by examining octanoate analog 17 (Table 1), containing an aliphatic chain that could participate in hydrophobic packing but lacked a conjugated ring system. This compound remained a potent agonist, albeit with 10-fold higher EC₅₀ value compared with TP1. Next, we sought to determine if truncated TP analogs could still elicit LasR agonism, so an acetate group was appended to the R₂ position (18). Despite this group's inability to participate in hydrophobic packing, it was surprisingly a full agonist of LasR (96% max activity) with about 20-fold reduced potency compared with TP1. To determine the importance of the ester, we prepared and tested methoxymethyl ether (19) and methyl ether (20) derivatives, which also maintained full agonism of LasR but lost ~40- to >60-fold-potency relative to TP1. The largest loss in potency resulted from an analog containing an unfunctionalized phenol (R₂ = H, 21), which exhibited a >900-fold loss in potency. Together, these data demonstrate that the hydrophobic contacts made by the ester aryl ring of TP1 have a significant impact on compound potency but are not essential for full agonism of LasR. Further, we reason that removal of TP1's phenyl ring in compounds 18–21 would leave significant empty space in the ligand-binding site of LasR (assuming these derivatives target the same site), which motivates the question of how LasR's structure is capable of both accommodating these sterically smaller ligands while activating transcription to levels analogous to the larger ligands. We return to this question below.

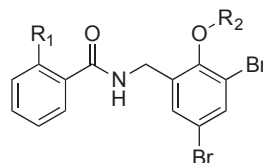
In Vitro Calorimetric Analyses Corroborate Compound Activity Trends from Cell-Based Reporter Assays

Cell-based reporter assays provide convenient platforms to analyze the SAR of LuxR-type receptor modulators, and these assays also indicate that active molecules are likely cell permeable. However, when possible, it is best to have a secondary *in vitro* assay to demonstrate direct molecular interactions between the LuxR-type receptor and the small molecule of interest. That said, *in vitro* assays have traditionally been problematic with many LuxR-type receptors, again due to the low stability of the receptor in the presence of antagonists (Welsh and Blackwell, 2016b). We wanted to circumvent this challenge in the current study, as we had chosen to study LasR agonists instead. Gratifyingly, we were able to express and purify the LasR-LBD in the presence of each member of our focused TP-type library to probe receptor:ligand interactions using differential scanning fluorimetry (DSF; see Supplemental Information for methods) (Pantoliano et al., 2001; Vivoli et al., 2014). This method allows for investigation of the stability of a protein complex *in vitro*, and allowed us to calculate thermal transition midpoints (i.e., T_m values) for the unfolding of the different LasR-LBD:ligand



Scheme 1. Optimized Synthetic Route toward the Triphenyl Scaffold

Table 1. Structures of the TP1 Analog Library and Their Associated (1) EC₅₀ and Maximum Efficacy Data in the *E. coli* LasR Reporter Strain, (2) Thermal Melt Data in the Presence of LasR LBD, and (3) Structural Data in Complex with the LasR LBD (Buried Surface Area)



Compound	R ₁	R ₂	EC ₅₀ (nM) ^a	95% CI (nM) ^b	Maximum Efficacy ^c	Thermal Transition Midpoint	Buried Surface Area (Å ²) ^d
1 (OdDHL)	NA	NA	1.78	1.34–2.36	98%	–	
2 (TP-1)	NO ₂	-CO-2-Cl-phenyl	0.92	0.65–1.31	98%	70.5 ± 0.3	652
10	NO ₂	-CO-phenyl	1.16	0.89–1.52	100%	63.5 ± 0.3	633
11	NO ₂	-CO-2-NO ₂ -phenyl	0.67	0.53–0.86	93%	69.3 ± 0.3	655
12	NO ₂	-CO-2-OCH ₃ -phenyl	1.10	0.96–1.26	94%	68.9 ± 0.3	660
13	NO ₂	-CO-2-CN-phenyl	5.64	3.89–8.18	99%	64.5	655
14	NO ₂	-CO-4-Cl-phenyl	2.09	1.58–2.77	94%	66	655
15	NO ₂	-CO-4-Br-phenyl	1.62	1.24–2.11	91%	65.9 ± 0.5	659
16	NO ₂	-CO-4-OCH ₃ -phenyl	9.20	6.57–12.9	105%	63.7	668
17	NO ₂	-CO-(CH ₂) ₆ CH ₃	12.2	8.55–17.4	99%	65.4	689
18	NO ₂	-CO-CH ₃	20.5	16.6–25.3	96%	54.8 ± 0.3	
19	NO ₂	-CH ₂ OCH ₃	37.6	30.0–47.0	90%	57.2	537
20	NO ₂	-CH ₃	>60	–	85% ^e	56	
21	NO ₂	-H	>900	–	65% ^e	50.5 ± 0.5	
22	Cl	-CO-2-NO ₂ -phenyl	5.12	3.32–7.88	101%	62.6 ± 0.2	
23	Cl	-CO-2-Cl-phenyl	7.99	5.81–11.0	98%	64.3	

^aCalculated based on testing the compound's ability to activate LasR's transcriptional regulation of *lasI-lacZ* over a range of concentrations.

^bCI = 95% confidence interval for EC₅₀ values.

^cDenotes the highest amount of LasR activity observed at any concentration. Error = ±5%.

^dThe buried surface area (BSA) of each ligand:LasR-LBD structure was calculated using the PDBePISA web tool (<http://www.ebi.ac.uk/pdbe/pisa/>).

^eCompound insolubility precluded testing at higher concentrations; EC₅₀ shown constitutes a minimal value.

complexes (Table 1). While such measurements do not provide a direct thermodynamic measure of ligand affinity, comparison of melting profiles directly reflects relative binding affinities.

We observed that the T_m values for the LasR-LBD:ligand complexes could be correlated with either weak or strong agonism by the compound in the reporter assay. Specifically, more potent ligands ($EC_{50} \leq 12.2$ nM; **2**, **10–17**, **22**, and **23**) yielded ligand-bound complexes with a 10°C higher average T_m value (~65 °C) than less potent ligands ($EC_{50} \geq 20.5$ nM (**18–21**); average T_m value ~55°C). These T_m values are consistent with a model in which the more potent ligands enhance LasR-LBD thermostability more than the less potent ligands. In addition, the results of this secondary assay suggest that the compound activity measured indirectly in the cell-based reporter assay is likely produced through direct LasR:ligand interactions instead of a different, indirect mechanism.

Structural Analyses Reveal that LasR Agonists Cause Main Chain Structural Changes in the L3 Loop

We next sought to explore whether the different potencies and T_m values for individual ligands could correlate to structural changes in the LasR-LBD:ligand complexes. As crystallization of full-length LasR has proven challenging (Bottomley et al., 2007; Zou and Nair, 2009), we focused our efforts on solving

co-crystal structures with the LasR-LBD, and we were able to determine high-resolution structures with compounds **10–17** and **19** (see Supplemental Information for methods). Notably, the EC₅₀ values for these compounds in the reporter assay spanned three orders of magnitude (0.67–37.6 nM), so we were hopeful that these co-crystal structures could illuminate differences in the LasR-LBD structures that reflect their different levels of potency. The high Bragg resolution limit of each of the resultant structures (between 1.63 and 1.90 Å), the low coordinate errors derived from Luzzati plots of the raw data, and the multiple, crystallographically independent copies of the observed structures in crystals of each complex provide strong evidence that the differences are not due to adventitious crystallographic packing or spurious electron density features.

The overall fold of the LasR-LBD complexed to each of these nine different compounds recapitulates the architecture observed for the LasR-LBD in previous studies (Figure 2A) (Bottomley et al., 2007; Zou and Nair, 2009); however, certain compounds produced a significant deviation from prior structures at a loop encompassing residues Leu-40 to Phe-51, previously termed the L3 loop (Figures 2B and 2C) (Zou and Nair, 2009). This region of the LasR-LBD has been previously proposed to act as a “cap” for its ligand-binding pocket and packs closely against the ligand to form a solvent occluded

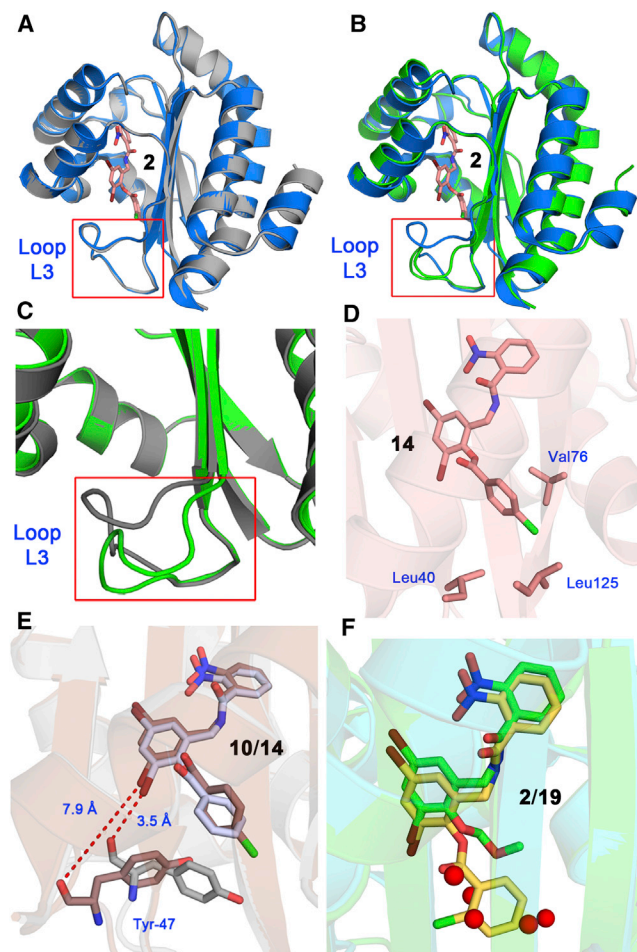


Figure 2. Selected Views of the LasR-LBD Structure with Various Ligands

(A) Superposition of structures of LasR-LBD:TP1 (**2**) (blue with structure of TP1 (**2**) shown in stick mode) and LasR-LBD:**10** (gray). Both complexes have the L3 loop “in.”

(B) Superposition of structures of LasR-LBD:TP1 (**2**) (blue with structure of TP1 (**2**) shown in stick mode) and LasR-LBD:**19** (green). LasR-LBD:**19** has the L3 loop “out.”

(C) Closer view of the superposition of the L3 loop region of structures of LasR-LBD:**10** (gray) and LasR-LBD:**19** (green).

(D) View of the ligand-binding site of the LasR-LBD:**14** (peach) structure; **14** is represented in stick mode.

(E) Superposition of the ligand-binding sites of LasR-LBD:**10** (gray) and LasR-LBD:**14** (brown) structures, showing the distances between the carbonyl oxygen of Tyr-47 and the corresponding bromine atoms.

(F) Superposition of the ligand-binding sites of LasR-LBD:**2** (protein in cyan and ligand in yellow orange) and LasR-LBD:**19** (green) structures, with the water molecules from LasR-LBD:**19** structure shown in red spheres.

hydrophobic core (Bottomley et al., 2007; Zou and Nair, 2009). We observed two disparate conformers of this region: one with the L3 loop folded “in” toward the ligand-binding pocket (Figure 2A, analogous to prior structures) and the other in which the loop was positioned away from the pocket, pointing “out” toward bulk solvent (Figures 2B and 2C). The co-crystal structures that closely recapitulate the L3-loop position of prior LasR-LBD structures were observed for compounds **10–13**.

These compounds were either unsubstituted (**10**) or 2-substituted (**11–13**) on the third aryl ring, making them very close mimics of TP1 (**2**). Thus, there is close structural similarity of LasR-LBD bound to **10–13** when compared with LasR-LBD:TP1 (RMSD of 0.46, 0.44, 0.51, and 0.57 Å, respectively). Indeed, the volumes of the ligand-binding pocket in each of these structures fall within the range of 906–1031 Å³, which is comparable with the volume of 909 Å³ observed in the TP1 co-crystal structure.

In contrast, compounds with 4-substitution on the third aryl ring (**14–16**) or a long alkyl chain (**17**) produced co-crystal structures with the alternate “out” L3 loop position, suggesting that the loop may be forced away from the ligand-binding pocket to accommodate their larger steric footprints relative to compounds more similar to TP1. The 4-substituents of these compounds have hydrophobic interactions with side chains (i.e., Leu-40, Val-76, Leu-125; Figure 2D) that are seemingly unimportant for binding 2-substituted TP analogs, and these alternate contacts may delay the maintenance of their LasR agonism efficacies (Table 1). One particularly striking structural shift that demonstrates the significant change in the L3 loop position concerns Tyr-47, which has been proposed to interact via its backbone carbonyl with one of the bromine substituents on the central ring of TP-type compounds to shield the ligand-binding pocket from water (Zou and Nair, 2009). When the loop is shifted toward the ligands (as in compounds **10–13**), the distance between the carbonyl oxygen of Tyr-47 and one of the bromine substituents is 3.5–3.9 Å compared with 7.8–8.2 Å when the loop is shifted out from the ligand-binding pocket as in compounds **14–17** (overlay of LasR with **10** and **14** shown in Figure 2E). This outward movement of the L3 loop increases the volume of the ligand-binding pocket for compounds **14–17**, ranging from 1037 to 1250 Å³.

The disposition of the L3 loop results in ligand-binding pockets of variable sizes, and to some extent, the surface area buried by the ligand (Table 1) may be used as a proxy for favorable protein-ligand interactions, provided that a given ligand does not compromise van der Waals contacts across the entire ligand-binding pocket. For example, even though the structure with benzoate analog **10** shows an inward L3 loop position for LasR, the lack of substituents on this ligand results in smaller buried surface area (633 Å³) than with any of the 2-substituted derivatives **11–13** (655–660 Å³). Consequently, compound **10** shows a slightly lower T_m value of ~64°C. Likewise, the structure of LasR-LBD bound to truncated analog **19** is also notable. This derivative of TP1 lacks the third aryl ring (Table 1), making it roughly 20% smaller than the other ligands, and we observed it to be an almost full agonist of LasR albeit with only modest potency (see above). Interestingly, the co-crystal structure of LasR-LBD:**19** revealed an “out” conformation of the L3 loop. Interaction of LasR with **19** buries only 538 Å³ of surface area. Perhaps as a consequence of orienting this smaller ligand, we observed additional solvent molecules in the hydrophobic binding pocket (overlay of LasR:**19** and LasR:TP1 (**2**) shown in Figure 2F). The presence of solvent in this unfilled pocket may destabilize the overall folding of LasR and could factor into the lower potency of **19** relative to the other L3 compounds that we were able to co-crystallize with the receptor. In addition, the LasR-LBD:**19** structure demonstrates that the two distinct

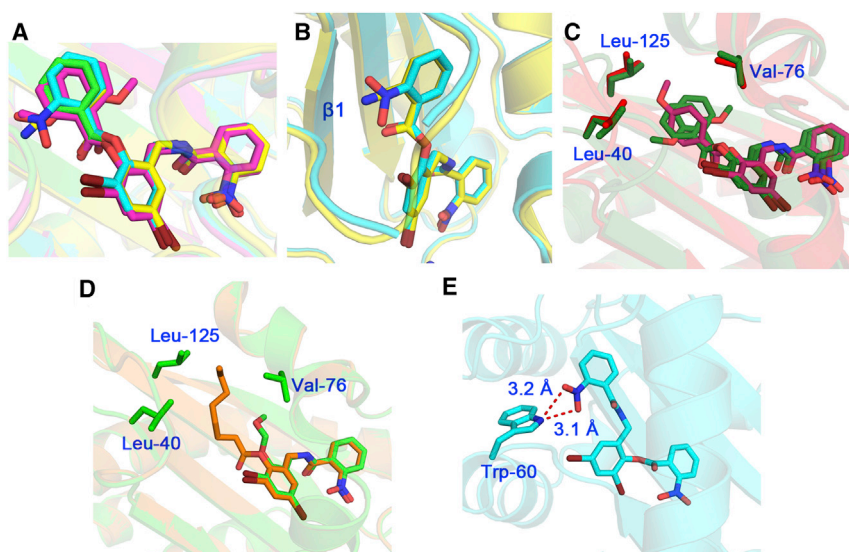


Figure 3. Selected Views of Ligands Bound to LasR-LBD

(A) Superposition of the ligand-binding sites of LasR-LBD:**10–13** structures (green, cyan, purple, and yellow, respectively).

(B) Superposition of the ligand-binding sites of LasR-LBD:**11** (cyan) and LasR-LBD:**13** (yellow) structures. The $\beta 1$ strand of LasR-LBD structure is indicated.

(C) Superposition of the ligand-binding sites of LasR-LBD:**12** (forest green) and LasR-LBD:**16** (red) structures, with the Leu-40, Val-76, and Leu-125 side chains shown in sticks.

(D) Superposition of the ligand-binding sites of LasR-LBD:**17** (orange) and LasR-LBD:**19** (green) structures, with the Leu-40, Val-76, and Leu-125 side chains shown in sticks.

(E) The ligand-binding site of LasR-LBD:**11** (cyan) structure, showing the distances between the nitro oxygens of **11** and N ϵ 1 of Trp-60.

conformers of the L3 loop are related to both ligand size, as seems to be the case for **10–13** and **14–17**, and ligand potency, as observed for **19**. While structural data are not available for compounds **18**, **20**, and **21**, it is plausible that the lower T_m values measured with these ligands ($\sim 51^\circ\text{C}$ – 56°C) may be due to the lack of bulky substituents at position R2, which would similarly result in unfilled pockets in their respective crystals with LasR.

Structural Insights into Ligand Binding and Their Link to Compound Potency

We next scrutinized the binding modes of ligands **10–17** and **19** with the LasR-LBD in the co-crystal structures in more detail in order to gain possible insights into their potency differences. Overall, the poses of these molecules in the binding site were similar, and the only major differences were seen in the orientation of the aryl ring connected through the ester. Examining the unsubstituted phenyl (**10**) and 2-substituted phenyl compounds (**11–13**), the ester aryl rings are aligned in the same plane and almost perfectly overlay when disregarding their differing substituents (Figure 3A). 2-Nitrobenzoate analog **11** and 2-cyanobenzoate analog **13** each bound the LasR-LBD in a single orientation with their substituents facing the same direction, while 2-methoxybenzoate analog **12** displayed two conformers in the structure with the 2-methoxyl substituents in each conformer rotated 180° (Figure 3A). We were surprised that the potency of **13** as a LasR agonist is around 5-fold less than that of compounds **10–12**, despite a near identical superposition of these different ligand structures bound to the LBD. We speculate that the reduced potency of **13** could relate to its linear and polar 2-cyano substituent pointing toward hydrophobic β sheet 1 in LasR, as this interaction may result in weaker binding or structural destabilization (Figure 3B). There were no direct interactions between LasR and the substituent groups at the 2-position of the ester aryl ring for compounds **10–12**, which is consistent with these compounds displaying similar potencies (EC_{50} values between 0.67 and 1.16 nM) despite their different substituents.

We expected 4-substituted TP1 analogs **14–16** to be too long for productive binding in the LasR ligand-binding pocket, which

we postulated would perturb protein binding and/or folding. We were surprised that these compounds remained relatively potent agonists, albeit with 2- and 8-fold reduced potency when compared with their respective 2-substituted regioisomers **2** and **12**. In the co-crystal structures of **14–16**, their binding pose was modified relative to the 2-substituted analogs **11–13**, with the ester aryl ring rotating close to 90° compared with **11–13** (Figure 3C). 4-Methoxybenzoate analog **16** was the least potent LasR agonist of the 4-substituted analogs, and we propose that this may be due to the polar 4-methoxyl group of **8** pointing toward the aforementioned hydrophobic space in LasR composed of Leu-40, Val-76, and Leu-125 (Figure 3C), which may destabilize binding interactions.

Generally, “diphenyl” TP1 derivatives lacking the third phenyl ring lost appreciable potency compared with triphenyl compounds. However, in octanoate analog **17**, the third phenyl ring is replaced with an 8-carbon alkyl chain, and this ligand mimicked the potency of the triphenyl compounds in the reporter assay and by DSF. In the corresponding co-crystal structure with the LBD, the alkyl chain of **17** makes hydrophobic contacts in the region that the third aryl ring would normally occupy (Figure 3D). These contacts may serve as an anchor for **17** and enhance its binding to LasR; this rationale then would account for the lower potency of MOM ether analog **19** relative to **17**, as **19** possesses only a short methoxymethyl ether tail (Figure 3D). Acetate analog **18**, methyl ether analog **20**, and phenol analog **21** also lack this alkyl anchor group. While we lack structural data for these three compounds in complex with the LasR-LBD, we hypothesize that they likely bind in an analogous manner as **19**. The loss of the alkyl anchor groups in compounds **18**, **20**, and **21** would spare more space for accessible water molecules in the binding pockets, and solvent molecules can be observed within hydrogen-bonding distance in the structure with **19** (Figure 2F). Bound solvent may lead to the reduced potencies of some of these compounds in the reporter assay and lower T_m values. Lastly, in 2-nitrobenzoate analog **22** and 2-chlorobenzoate analog **23**, the R1 group was switched to chloro from nitro to compare with 2-nitrobenzoate **11** and 2-chlorobenzoate **2**

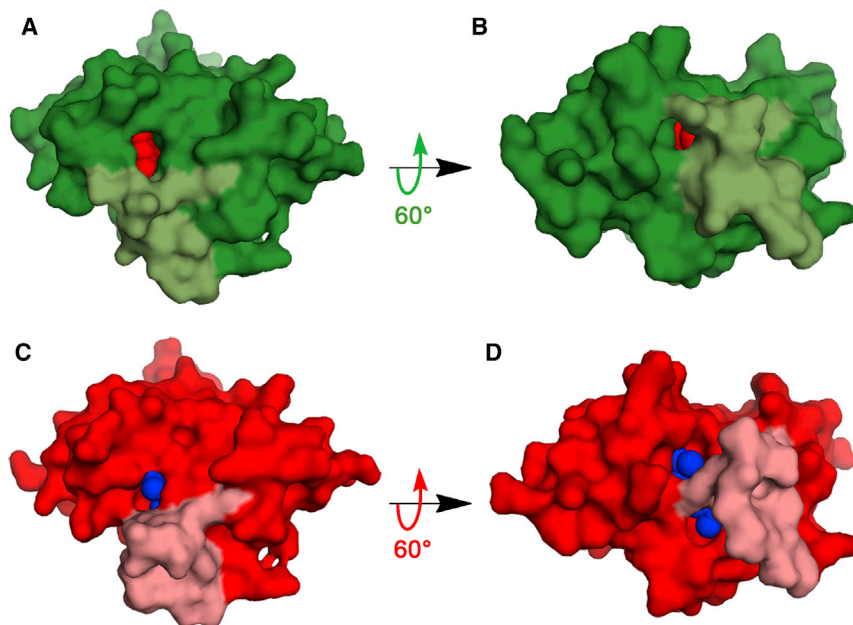


Figure 4. Molecular Surface Views of LasR-LBD Structures

(A) Molecular surface view of LasR-LBD:**12** structure (forest green) with L3 loop in light green and ligand in red.

(B) 60° rotation of view in part (A) showing the front side of L3 loop.

(C) Molecular surface view of LasR-LBD:**16** structure (red) with L3 loop in pink and ligand in blue.

(D) 60° rotation of view in part (C) showing the front side of L3 loop.

(**TP1**), respectively, and their potencies decreased about 7-fold. Previous structural studies of LasR-LBD:**TP1** showed that the replacement of a nitro group with chloride results in a loss of one of the two hydrogen bonds between the nitro group and Nε1 of Trp-60 (Zou and Nair, 2009); these two hydrogen bonds are also apparent in the structure of LasR-LBD:**11** (Figure 3E). We suspect that the loss of these hydrogen bonds to LasR is a factor in the reduced potencies of **22** and **23**. Collectively, these structural studies provide a significantly expanded molecular view of how TP-type compounds bind to the LasR-LBD.

L3 Loop Flexibility Provides a Mechanism for Ligand Exchange

Based on *in vitro* studies, many members of the LuxR-type protein family were originally believed to require native ligand (or agonist) binding during protein translation for proper polypeptide folding to occur (Schuster et al., 2004; Zhu and Winans, 1999, 2001). However, this may not hold true for all LuxR receptors, as low levels of folded LasR have been shown to be present in heterologous expression systems even in the absence of ligand (Sappington et al., 2011). Nevertheless, the mechanism by which ligands can exchange within the LasR-binding site remains unclear, as highly potent ligands such as OdDHL (**1**) or **TP1** (**2**) are almost fully encapsulated within the ligand-binding pocket (see also compound **12**, Figure 4A). This encasement is partially due to the orientation of the L3 loop that caps the ligand-binding pocket. However, the structural studies described here show that when LasR binds to a subset of compounds (such as 4-methoxybenzoate analog **16** or MOM ether analog **19**), the L3 loop is shifted out toward bulk solvent, resulting in a much more open binding pocket (Figure 4B). Again, to some degree, the extent of the surface area buried when each of the respective compounds are engaged in the binding pocket is reflected in the corresponding T_m values, as well as the EC_{50} for these ligands, with the caveats stated previously (Table 1). These data are consistent with a model in which the L3 loop serves as a molec-

ular gate to dynamically open and close the LasR-binding pocket to provide ligand entry. The resultant pocket encapsulates ligands of suitable steric and electronic constraints to afford tight binding, whereas those that fail to meet such constraints generally show decreased potency. The dynamics of the L3 loop may also explain why the production and purification of LasR in the absence of bound

ligands has been challenging (Sappington et al., 2011; Schuster et al., 2004; Zhu and Winans, 1999, 2001).

Movement of the L3 Loop May Affect the Conformation of the LBD and LBD:DBD Contacts

To further explore the relevance of the observed changes to the LasR-LBD structure upon binding various TP-type ligands of varying potency, and in lieu of a full-length LasR crystal structure, we mapped these changes onto a full-length structure of another homologous LuxR-type protein found in *P. aeruginosa*, QscR. QscR responds to the same native ligand as LasR (OdDHL, **1**), and the structure of full-length QscR bound to OdDHL has been previously determined (Lintz et al., 2011). The QscR-LBD is the most similar structure to LasR-LBD (RMSD of 3.3 Å, for 142 aligned C α atoms), and the L3 loop of both structures is located in similar positions (Figure 5). Notably, superimposition of the QscR and LasR-LBD structures demonstrates that the L3 loop of each protein exists close to the interface between the LBD and the DBD in QscR. Structures of LasR-LBD bound with compounds **10–13** possess the “in” conformation for L3 loop, and those in complex with compounds **14–17** and **19** represent the “out” conformation for L3 loop. These two observed conformations of the L3 loop in crystal structures may represent dynamic movement and flexibility in response to the binding of ligands with various sizes and potencies. The subtle movement and flexibility of the L3 loop may be further involved in transducing ligand binding to structural changes in the DBD, which would configure the receptor for dimerization, DNA binding, and transcriptional regulation in the presence of these ligands. Subtle conformation changes in the LBD resulting in dramatic DBD movement was previously noticed when comparing the CviR structure in complex with a synthetic antagonist (a chlorolactone compound, CL) and a close homolog structure (CviR') in complex with an agonist (*N*-hexanoyl HL; C6-AHL) (Chen et al., 2011). The LBDs of the CviR':C6-AHL and CviR:CL structures are very similar (RMSD

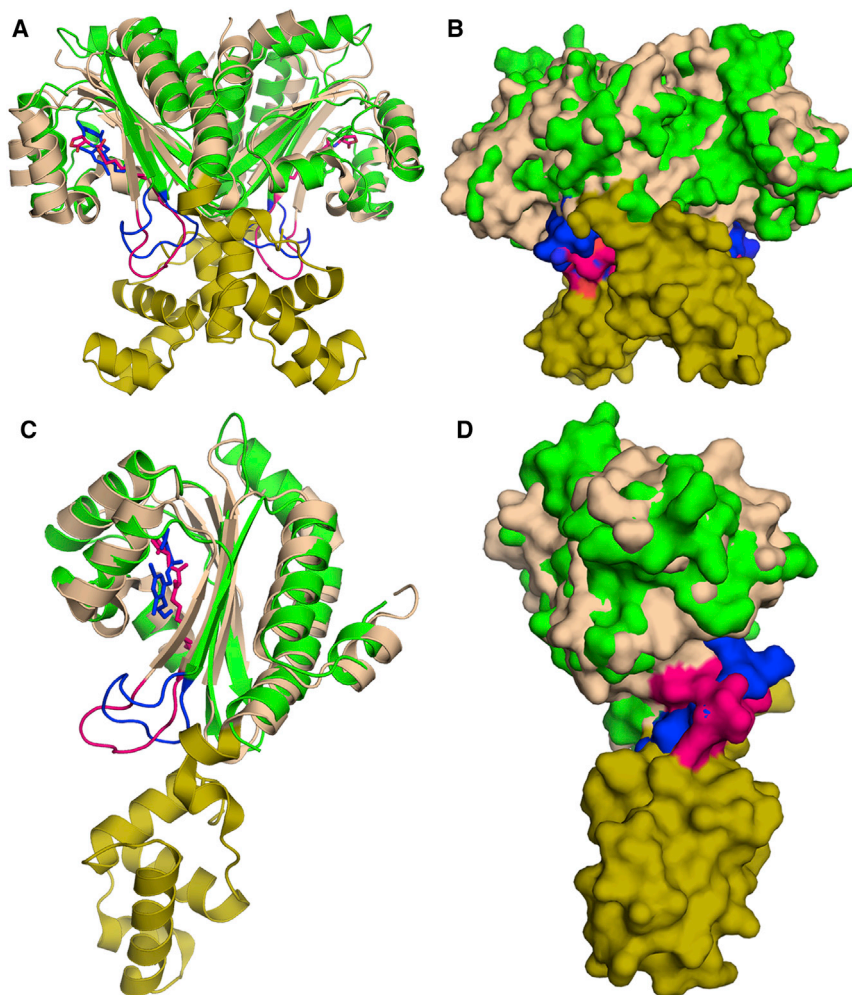


Figure 5. Overlay Views of the LasR-LBD:19 Structure onto a Full-Length LuxR-Type Receptor Structure

(A) Superposition of the dimer structures of LasR-LBD:19 and QscR:OdDHL (1), with LasR-LBD:19 in green, LasR-LBD L3 loop and structure of 19 in blue, QscR-LBD in wheat, QscR-DBD in olive, and QscR L3 loop and structure of OdDHL in hot pink. (B) Molecular surface view of the dimer structures of LasR-LBD:19 and QscR:OdDHL after superposition.

(C) Superposition of the monomer structures of LasR-LBD:19 and QscR:OdDHL.

(D) Molecular surface view of the monomer structure of LasR-LBD:19 and QscR:OdDHL after superposition.

Colors in (B)–(D) match those in (A).

of 0.94 Å, for 164 aligned C α atoms), yet their DBDs possess distinct orientations of $\sim 10^\circ$.

DISCUSSION

We postulated that study of LasR in complex with agonist ligands of varying potencies could provide insights into the molecular mechanisms of its activation and inactivation by non-native ligands. We developed a highly efficient route for the synthesis of TP ligands that will accelerate analog development in the future, and identified a series of SAR data for LasR agonism by this ligand class using cell-based reporter assays. Chiefly, these SAR data demonstrated that the TP aryl ester ring is not necessary for maximal activation of LasR, as TP ligands with (1) modifications to the phenyl substituents (10–16), (2) phenyl replacement with an alkyl chain (17), and (3) truncations of the phenyl ring (18–20) were able to elicit full or very close to full LasR agonism, albeit with minor to significant reductions in potency. We also discovered that the thermal stability of the LasR-LBD when bound to these ligands (as reported *in vitro* by DSF) largely increased with ligand potency (as reported in the cell-based assays), supporting a mechanism by which increased stabilization of LasR in cells is a cause for

increased ligand potency. Our structural results with a series of TP-derived ligands of differing potencies bound to the LasR-LBD provide significance for the L3 loop, which has previously been viewed as a domain that non-specifically contacts ligands. Based on our studies, movement of the L3 loop results in a change in the volume of the binding pocket, and ligands that are fully encapsulated in the resultant pocket can demonstrate stronger LasR agonism. We note that each of the structures reported herein contain multiple, independent copies of the LasR ligand complex in the crystallographic asymmetric unit, each of which contain a consistent orientation of L3, arguing against crystal-lattice artifacts.

Taken together, our results allowed us to put forth a model for LasR activity where the L3 loop dynamically opens and closes, and in the absence of productive ligand binding, would allow solvent into the hydrophobic ligand-binding pocket leading to destabilization and unfolding. However, in complexes with ligand bound, this loop is held in a conformation that simultaneously seals the ligand-binding pocket from solvent and provokes structural changes to the DBD toward transcriptional activation. Such a mechanism is congruent with the data reported here for at least the TP ligand class; additional studies are of course warranted to examine if this mechanism is also operative for different LasR ligand classes (such as AHLs) and for different LuxR-type receptors.

Recently, Kim et al. (2017) reported the crystal structure of the LBD of AHL-bound and apo YenR, a LuxR-type receptor from the enteropathogen *Yersinia enterocolitica*. In these structures, the largest modifications between ligand-bound and apo YenR include (1) significant movement of a loop between Gly-129 and Ser-132 (distinct from the L3 loop) and (2) closing of the ligand channel by way of a conformational shift of Phe-98. Beyond those changes, the tertiary structures could be closely superimposed when comparing ligand-bound and apo YenR. These findings with YenR, albeit for a different structural loop,

provide general support for the plausibility of our mechanism for ligand recognition in LasR.

The results of this study are significant for several reasons. First, we have further underscored the value of the TP ligand class as a versatile and tunable scaffold for LasR agonist design. Second, we have demonstrated that our reporter assay data corroborate the thermal stability data trends for the ligands reported herein. Comparison of cell-based and *in vitro* assay data for synthetic LuxR-type receptor ligands is rare, as again these receptors are difficult to manipulate *in vitro*. Third, we have provided a considerable number of co-crystal structures (nine in total) for the LasR-LBD bound to non-native ligands. In view of the growing interest in the TP scaffold (Capilato et al., 2017; O'Brien et al., 2015; O'Reilly and Blackwell, 2016) and QS in *P. aeruginosa* in general (Papenfort and Bassler, 2016; Welsh and Blackwell, 2016b), these structures are of fundamental interest. Fourth, we propose a mechanism for LasR activation and signal transduction that implicates the L3 loop as a possible gatekeeper for productive protein folding, dynamically opening and closing in the absence of ligand to provide entry to the ligand-binding pocket. Notably, these insights were made possible by the study of a series of receptor agonists of differing potencies. We believe that this approach focused on receptor *agonism*, as opposed to *antagonism*, could be particularly useful for the biophysical study of LuxR-type proteins in view of the challenges of manipulating them *in vitro*.

SIGNIFICANCE

Quorum sensing plays a prominent role in the virulence of *P. aeruginosa* and other common bacterial pathogens, and methods to circumvent this cell-cell signaling network have attracted interest as a route to block infection. Synthetic molecules have been developed that antagonize the LasR receptor, yet the modes by which these compounds interact with LasR are largely unknown. A detailed understanding of the ligand:receptor interface and structural changes that occur upon binding would transform the development of ligands to target this receptor. The instability of LasR (and other related LuxR-type homologs), however, in the presence of antagonists has thwarted such investigations. The current study pivoted the focus from LasR antagonists to LasR agonists of varied potencies, as we reasoned that studying a spectrum of LasR:agonist complexes could provide a portal into the mechanisms by which this receptor interacts with non-native ligands, while maintaining sufficient protein stability for *in vitro* work. A focused library of agonist ligands based on a known triphenyl ligand scaffold were efficiently synthesized, characterized for LasR activation using cell-based and *in vitro* assays, and submitted to X-ray crystallography in complex with the LasR ligand-binding domain. The collective results revealed a likely functional role for the L3 loop, which in prior studies had been implicated in non-specific interactions with ligand. Our studies identify that this loop can adopt different conformations, and ligands that are poised for optimal contacts with the resultant binding pocket show greater agonism than those that are not. These data for the L3 loop prompt a proposal for LasR ligand recognition and subsequent activation, and

suggest a plausible pathway by which agonists stabilize and antagonists destabilize LasR, respectively. Moreover, this work provides a basis for next-generation LasR ligand design that specifically optimizes contact with the receptor in light of the L3 loop conformation.

STAR★METHODS

Detailed methods are provided in the online version of this paper and include the following:

- KEY RESOURCES TABLE
- CONTACT FOR REAGENTS AND RESOURCE SHARING
- EXPERIMENTAL MODEL AND SUBJECT DETAILS
 - Microbe Strains
- METHODS DETAILS
 - Chemical Synthesis
 - LasR β -Galactosidase Activity Assay
 - Differential Scanning Fluorimetry Assay Protocol
 - Purification and Crystallization of LasR-LBD:Compound Complexes
 - Data Collection, Structure Determination, and Refinement
- QUANTIFICATION AND STATISTICAL ANALYSIS
- DATA AND SOFTWARE AVAILABILITY

SUPPLEMENTAL INFORMATION

Supplemental Information includes one figure, one table, and two data reports and can be found with this article online at <https://doi.org/10.1016/j.chembiol.2018.06.007>.

ACKNOWLEDGMENTS

Financial support for this work was provided by the NIH (R01 GM109403 to H.E.B.). M.C.O. acknowledges support from the Arnold and Mabel Beckman Foundation through an Arnold O. Beckman Postdoctoral Fellowship. NMR and MS instrumentation at UW-Madison are supported by the NSF (CHE-1048642 and CHE-0342998) and the NIH (1S10 OD020022), respectively, and a generous gift from Paul J. Bender. We thank Keith Brister and colleagues for facilitating data collection at LS-CAT (Argonne National Labs, IL).

AUTHOR CONTRIBUTIONS

M.C.O., S.D., S.K.N., and H.E.B. designed the study. M.C.O., F.M.R., K.M.K., and R.S.K. performed the chemical synthesis and microbiology experiments. S.D. and S.K.N. performed the structural biology and biochemistry experiments. All authors analyzed the experimental data, and M.C.O., S.D., S.K.N., and H.E.B. wrote the manuscript.

DECLARATION OF INTERESTS

The authors declare no competing interests.

Received: September 21, 2017

Revised: February 27, 2018

Accepted: June 20, 2018

Published: July 19, 2018

REFERENCES

Amara, N., Krom, B.P., Kaufmann, G.F., and Meijler, M.M. (2011). Macromolecular inhibition of quorum sensing: enzymes, antibodies, and beyond. *Chem. Rev.* **111**, 195–208.

- Amara, N., Mashiach, R., Amar, D., Krief, P., Spieser, S.A., Bottomley, M.J., Aharoni, A., and Meijler, M.M. (2009). Covalent inhibition of bacterial quorum sensing. *J. Am. Chem. Soc.* *131*, 10610–10619.
- Asfahl, K.L., and Schuster, M. (2018). Additive effects of quorum sensing anti-activators on *Pseudomonas aeruginosa* virulence traits and transcriptome. *Front. Microbiol.* *8*, 2654.
- Bottomley, M.J., Muraglia, E., Bazzo, R., and Carfi, A. (2007). Molecular insights into quorum sensing in the human pathogen *Pseudomonas aeruginosa* from the structure of the virulence regulator LasR bound to its autoinducer. *J. Biol. Chem.* *282*, 13592–13600.
- Caddick, S., Judd, D.B., Lewis, A.K.D., Reich, M.T., and Williams, M.R.V. (2003). A generic approach for the catalytic reduction of nitriles. *Tetrahedron* *59*, 5417–5423.
- Capilato, J.N., Philippi, S.V., Reardon, T., McConnell, A., Oliver, D.C., Warren, A., Adams, J.S., Wu, C., and Perez, L.J. (2017). Development of a novel series of non-natural triaryl agonists and antagonists of the *Pseudomonas aeruginosa* LasR quorum sensing receptor. *Bioorg. Med. Chem.* *25*, 153–165.
- Chen, G., Swem, L.R., Swem, D.L., Stauff, D.L., O'Loughlin, C.T., Jeffrey, P.D., Bassler, B.L., and Hughson, F.M. (2011). A strategy for antagonizing quorum sensing. *Mol. Cell* *42*, 199–209.
- Chugani, S.A., Whiteley, M., Lee, K.M., D'Argenio, D., Manoil, C., and Greenberg, E.P. (2001). QscR, a modulator of quorum-sensing signal synthesis and virulence in *Pseudomonas aeruginosa*. *Proc. Natl. Acad. Sci. USA* *98*, 2752–2757.
- Churchill, M.E.A., and Chen, L. (2011). Structural basis of acyl-homoserine lactone-dependent signaling. *Chem. Rev.* *111*, 68–85.
- Galloway, W.R., Hodgkinson, J.T., Bowden, S., Welch, M., and Spring, D.R. (2012). Applications of small molecule activators and inhibitors of quorum sensing in Gram-negative bacteria. *Trends Microbiol.* *20*, 449–458.
- Galloway, W.R., Hodgkinson, J.T., Bowden, S.D., Welch, M., and Spring, D.R. (2011). Quorum sensing in gram-negative bacteria: small-molecule modulation of AHL and AI-2 quorum sensing pathways. *Chem. Rev.* *111*, 28–67.
- Gerdt, J.P., and Blackwell, H.E. (2014). Competition studies confirm two major barriers that can preclude the spread of resistance to quorum-sensing inhibitors in bacteria. *ACS Chem. Biol.* *9*, 2291–2299.
- Gerdt, J.P., McInnis, C.E., Schell, T.L., Rossi, F.M., and Blackwell, H.E. (2014). Mutational analysis of the quorum-sensing receptor LasR reveals interactions that govern activation and inhibition by nonlactone ligands. *Chem. Biol.* *21*, 1361–1369.
- Geske, G.D., O'Neill, J.C., Miller, D.M., Mattmann, M.E., and Blackwell, H.E. (2007). Modulation of bacterial quorum sensing with synthetic ligands: systematic evaluation of *N*-acylated homoserine lactones in multiple species and new insights into their mechanisms of action. *J. Am. Chem. Soc.* *129*, 13613–13625.
- Griffith, K.L., Shah, I.M., Myers, T.E., O'Neill, M.C., and Wolf, R.E., Jr. (2002). Evidence for "pre-recruitment" as a new mechanism of transcription activation in *Escherichia coli*: the large excess of SoxS binding sites per cell relative to the number of SoxS molecules per cell. *Biochem. Biophys. Res. Commun.* *291*, 979–986.
- Hodgkinson, J.T., Galloway, W.R., Wright, M., Mati, I.K., Nicholson, R.L., Welch, M., and Spring, D.R. (2012). Design, synthesis and biological evaluation of non-natural modulators of quorum sensing in *Pseudomonas aeruginosa*. *Org. Biomol. Chem.* *10*, 6032–6044.
- Kim, Y., Chhor, G., Tsai, C.S., Fox, G., Chen, C.S., Winans, N.J., Jedrzejczak, R., Joachimiak, A., and Winans, S.C. (2017). X-ray crystal structures of the pheromone-binding domains of two quorum-hindered transcription factors, YenR of *Yersinia enterocolitica* and CepR2 of *Burkholderia cenocepacia*. *Proteins* *85*, 1831–1844.
- Lee, J.H., Lequette, Y., and Greenberg, E.P. (2006). Activity of purified QscR, a *Pseudomonas aeruginosa* orphan quorum-sensing transcription factor. *Mol. Microbiol.* *59*, 602–609.
- Lindsay, A., and Ahmer, B.M. (2005). Effect of SdiA on biosensors of *N*-acylhomoserine lactones. *J. Bacteriol.* *187*, 5054–5058.
- Lintz, M.J., Oinuma, K., Wysoczynski, C.L., Greenberg, E.P., and Churchill, M.E. (2011). Crystal structure of QscR, a *Pseudomonas aeruginosa* quorum sensing signal receptor. *Proc. Natl. Acad. Sci. USA* *108*, 15763–15768.
- Lyczak, J.B., Cannon, C.L., and Pier, G.B. (2000). Establishment of *Pseudomonas aeruginosa* infection: lessons from a versatile opportunist. *Microbes Infect.* *2*, 1051–1060.
- Mellbye, B., and Schuster, M. (2011). The sociomicrobiology of antivirulence drug resistance: a proof of concept. *MBio* *2*, <https://doi.org/10.1128/mBio.00131-11>.
- Moore, J.D., Rossi, F.M., Welsh, M.A., Nyffeler, K.E., and Blackwell, H.E. (2015). A comparative analysis of synthetic quorum sensing modulators in *Pseudomonas aeruginosa*: New insights into mechanism, active efflux susceptibility, phenotypic response, and next-generation ligand design. *J. Am. Chem. Soc.* *137*, 14626–14639.
- Müh, U., Hare, B.J., Duerkop, B.A., Schuster, M., Hanzelka, B.L., Heim, R., Olson, E.R., and Greenberg, E.P. (2006a). A structurally unrelated mimic of a *Pseudomonas aeruginosa* acyl-homoserine lactone quorum-sensing signal. *Proc. Natl. Acad. Sci. USA* *103*, 16948–16952.
- Müh, U., Schuster, M., Heim, R., Singh, A., Olson, E.R., and Greenberg, E.P. (2006b). Novel *Pseudomonas aeruginosa* quorum-sensing inhibitors identified in an ultra-high-throughput screen. *Antimicrob. Agents Chemother.* *50*, 3674–3679.
- O'Brien, K.T., Noto, J.G., Nichols-O'Neill, L., and Perez, L.J. (2015). Potent irreversible inhibitors of LasR quorum sensing in *Pseudomonas aeruginosa*. *ACS Med. Chem. Lett.* *6*, 162–167.
- O'Loughlin, C.T., Miller, L.C., Siryaporn, A., Drescher, K., Semmelhack, M.F., and Bassler, B.L. (2013). A quorum-sensing inhibitor blocks *Pseudomonas aeruginosa* virulence and biofilm formation. *Proc. Natl. Acad. Sci. USA* *110*, 17981–17986.
- O'Reilly, M.C., and Blackwell, H.E. (2016). Structure-based design and biological evaluation of triphenyl scaffold-based hybrid compounds as hydrolytically stable modulators of a LuxR-type quorum sensing receptor. *ACS Infect. Dis.* *2*, 32–38.
- Pantoliano, M.W., Petrella, E.C., Kwasnoski, J.D., Lobanov, V.S., Myslik, J., Graf, E., Carver, T., Asel, E., Springer, B.A., Lane, P., et al. (2001). High-density miniaturized thermal shift assays as a general strategy for drug discovery. *J. Biomol. Screen.* *6*, 429–440.
- Papenfort, K., and Bassler, B.L. (2016). Quorum sensing signal-response systems in Gram-negative bacteria. *Nat. Rev. Microbiol.* *14*, 576–588.
- Rutherford, S.T., and Bassler, B.L. (2012). Bacterial quorum sensing: its role in virulence and possibilities for its control. *Cold Spring Harb. Perspect. Med.* *2*, <https://doi.org/10.1101/cshperspect.a012427>.
- Sappington, K.J., Dandekar, A.A., Oinuma, K., and Greenberg, E.P. (2011). Reversible signal binding by the *Pseudomonas aeruginosa* quorum-sensing signal receptor LasR. *MBio* *2*, e00011-11.
- Schuster, M., Sexton, D.J., Diggle, S.P., and Greenberg, E.P. (2013). Acyl-homoserine lactone quorum sensing: From evolution to application. *Annu. Rev. Microbiol.* *67*, 43–63.
- Schuster, M., Urbanowski, M.L., and Greenberg, E.P. (2004). Promoter specificity in *Pseudomonas aeruginosa* quorum sensing revealed by DNA binding of purified LasR. *Proc. Natl. Acad. Sci. USA* *101*, 15833–15839.
- Smith, K.M., Bu, Y., and Suga, H. (2003a). Library screening for synthetic agonists and antagonists of a *Pseudomonas aeruginosa* autoinducer. *Chem. Biol.* *10*, 563–571.
- Smith, K.M., Bu, Y.G., and Suga, H. (2003b). Induction and inhibition of *Pseudomonas aeruginosa* quorum sensing by synthetic autoinducer analogs. *Chem. Biol.* *10*, 81–89.
- Suneby, E.G., Herndon, L.R., and Schneider, T.L. (2017). *Pseudomonas aeruginosa* LasR.DNA binding is directly inhibited by quorum sensing antagonists. *ACS Infect. Dis.* *3*, 183–189.
- Vivoli, M., Novak, H.R., Littlechild, J.A., and Harmer, N.J. (2014). Determination of protein-ligand interactions using differential scanning fluorimetry. *J. Vis. Exp.* <https://doi.org/10.3791/51809>.

- Welsh, M.A., and Blackwell, H.E. (2016a). Chemical genetics reveals environment-specific roles for quorum sensing circuits in *Pseudomonas aeruginosa*. *Cell Chem. Biol.* *23*, 361–369.
- Welsh, M.A., and Blackwell, H.E. (2016b). Chemical probes of quorum sensing: From compound development to biological discovery. *FEMS Microbiol. Rev.* *40*, 774–794.
- Whiteley, M., Diggle, S.P., and Greenberg, E.P. (2017). Progress in and promise of bacterial quorum sensing research. *Nature* *551*, 313–320.
- Zakhari, J.S., Kinoyama, I., Struss, A.K., Pullanikat, P., Lowery, C.A., Lardy, M., and Janda, K.D. (2011). Synthesis and molecular modeling provide insight into a *Pseudomonas aeruginosa* quorum sensing conundrum. *J. Am. Chem. Soc.* *133*, 3840–3842.
- Zhu, J., and Winans, S.C. (1999). Autoinducer binding by the quorum-sensing regulator TraR increases affinity for target promoters *in vitro* and decreases TraR turnover rates in whole cells. *Proc. Natl. Acad. Sci. USA* *96*, 4832–4837.
- Zhu, J., and Winans, S.C. (2001). The quorum-sensing transcriptional regulator TraR requires its cognate signaling ligand for protein folding, protease resistance, and dimerization. *Proc. Natl. Acad. Sci. USA* *98*, 1507–1512.
- Zou, Y., and Nair, S.K. (2009). Molecular basis for the recognition of structurally distinct autoinducer mimics by the *Pseudomonas aeruginosa* LasR quorum-sensing signaling receptor. *Chem. Biol.* *16*, 961–970.

STAR★METHODS

KEY RESOURCES TABLE

REAGENT or RESOURCE	SOURCE	IDENTIFIER
Bacterial and Virus Strains		
<i>E. coli</i> JLD271	Ahmer lab	(Lindsay and Ahmer, 2005)
<i>E. coli</i> BL21 Star [™]	Nair lab	(Zou and Nair, 2009)
Chemicals, Peptides, and Recombinant Proteins		
Ampicillin	Sigma-Aldrich	A9518
3,5-dibromo-2-hydroxybenzotrile	Oakwood Chemical	034266
Gentamycin	Gold Biotechnology	G-400
Isopropyl β -D-1-thiogalactopyranoside (IPTG)	Gold Biotechnology	I2481
Kanamycin	Gold Biotechnology	K-120
Luria-Bertani (LB) medium	Research Products International	L24060
<i>N</i> -(3-oxo)-dodecanoyl L-homoserine lactone (OdDHL, 1)	Sigma-Aldrich	O9139
ortho-nitrophenyl- β -D-galactoside (ONPG)	Sigma-Aldrich	N1127
SYPRO Orange	Sigma-Aldrich	S5692
Deposited Data		
Crystal structure of LasR-LBD bound to 1	(Bottomley et al., 2007)	PDB: 2UV0
Crystal structure of LasR-LBD bound to 10	This paper	PDB: 6D6A
Crystal structure of LasR-LBD bound to 11	This paper	PDB: 6D6B
Crystal structure of LasR-LBD bound to 12	This paper	PDB: 6D6C
Crystal structure of LasR-LBD bound to 13	This paper	PDB: 6D6D
Crystal structure of LasR-LBD bound to 14	This paper	PDB: 6D6L
Crystal structure of LasR-LBD bound to 15	This paper	PDB: 6D6M
Crystal structure of LasR-LBD bound to 16	This paper	PDB: 6D6N
Crystal structure of LasR-LBD bound to 17	This paper	PDB: 6D6O
Crystal structure of LasR-LBD bound to 19	This paper	PDB: 6D6P
Recombinant DNA		
pSC11	Greenberg lab	(Chugani et al., 2001)
pJN105L	Greenberg lab	(Lee et al., 2006)
pET100/D TOPO	Nair lab	(Zou and Nair, 2009)
Software and Algorithms		
COOT	Crystallographic Object-Oriented Toolkit	https://www2.mrc-lmb.cam.ac.uk/personal/pemsley/coot/
GraphPad Prism (v. 6.0)	GraphPad Software, Inc.	https://www.graphpad.com/scientific-software/prism/
HKL2000	HKL Research, Inc.	http://www.hkl-xray.com/
Mestrenova	Mestrelab Research S. L.	http://mestrelab.com/
Phenix-Phaser	Python-based Hierarchical Environment for Integrated Xtallography	https://www.phenix-online.org/documentation/reference/phaser.html
Phenix-Refine	Python-based Hierarchical Environment for Integrated Xtallography	https://www.phenix-online.org/documentation/reference/refinement.html
CCP4-PROCHECK	Collaborative Computational Project No. 4 Software for Macromolecular X-Ray Crystallography	http://www.ccp4.ac.uk/html/procheck_man/index.html
Pymol	Schrödinger, LLC	https://pymol.org/2/
XDS Package	MPI for Medical Research	http://xds.mpimf-heidelberg.mpg.de/

CONTACT FOR REAGENTS AND RESOURCE SHARING

Further information and requests for resources and reagents should be directed to and will be fulfilled by the Lead Contact Helen Blackwell (blackwell@chem.wisc.edu).

EXPERIMENTAL MODEL AND SUBJECT DETAILS

Microbe Strains

Bacterial strain *E. coli* JLD271 with plasmids pJN105 (Arabinose-inducible expression vector for *lasR*; pBBRMCS backbone; Gentamycin^R) and pSC11 (Broad host range *lasI*-*lacZ* reporter; Ampicillin^R) was used in β -galactosidase assays. Freezer stocks were maintained at -80°C in Luria-Bertani (LB) medium and 50% glycerol. Bacterial overnight cultures were inoculated with single colonies that were isolated by streaking a freezer stock on an LB/agar (1.5%) plate with appropriate antibiotic supplements. The overnight cultures were grown in Erlenmeyer flasks or 13 mm X 100 mm test tubes in a standard laboratory incubator at 37°C with shaking (200 rpm) in LB medium (autoclave-sterilized). *E. coli* subcultures were grown in Erlenmeyer flasks. To minimize growth effects in 96-well plates, the following precautions were taken: (i) To reduce media evaporation, plates were incubated in stacks with "dummy plates" (containing sterile water in all wells) positioned on the top and bottom. Stacks of plates were placed in plastic containers to reduce air circulation. (ii) To reduce variation in ambient temperature, plates (including "dummy plates") were never stacked higher than six-fold.

Bacterial strain *E. coli* BL21 StarTM with plasmid pET100/D-TOPO was used for LasR-LBD production and stored at -80°C (Zou and Nair, 2009). The stock was used to inoculate 5 mL of LB medium for overnight growth at 37°C . A 2-L volume of LB medium supplemented with 50 $\mu\text{g}/\text{ml}$ kanamycin was inoculated with overnight culture and grown at 37°C until the OD_{600} reached 0.4. Thereafter, 1 mg of corresponding TP-type compound was added to the culture, and the culture was allowed to grow for 20 min more. The culture was then cooled in an ice water bath for 15 min, and protein production was induced via the addition of isopropyl β -D-1-thiogalactopyranoside (IPTG; final concentration of 0.5 mM). After overnight growth at 18°C , cells were harvested and resuspended in buffer containing 500 mM NaCl, 20 mM Tris (pH 8.0), and 10% glycerol. The resuspended cells were lysed by sonication and spun down by centrifugation, and the soluble supernatant was isolated.

METHODS DETAILS

Chemical Synthesis

All standard reagents and solvents were purchased from commercial sources (Sigma-Aldrich, TCI America, or Acros Organics) and used without further purification. Analytical thin-layer chromatography (TLC) was performed on 250 μm silica plates from Silicycle. Visualization was accomplished using UV light. Flash column chromatography was performed using Silica Gel 60 (230–400 mesh) from Macherey–Nagel. All ^1H - and ^{13}C -NMR spectra were recorded on a Bruker Avance-400 or -500 spectrometer. Chemical shifts are reported in ppm relative to residual solvent peaks as internal standards set to δ 7.26 and δ 77.16 (CDCl_3) or δ 2.50 and δ 39.52 ($(\text{CD}_3)_2\text{SO}$). NMR data are reported as follows: chemical shift, multiplicity (s = singlet, d = doublet, t = triplet, q = quartet, p = pentet, br = broad, dd = doublet of doublets, dq = doublet of quartets, td = triplet of doublets, pd = pentet of doublets, m = multiplet), coupling constant (Hz), and integration. High-resolution mass spectra (HRMS) were recorded on a Q Extractive Plus Orbitrap with an electrospray ion source. Further details of chemical syntheses, as well as compound characterization data by NMR and mass spectrometry, are available in [Data S1](#).

LasR β -Galactosidase Activity Assay

To evaluate the modulatory activities of compounds on LasR heterologously expressed in *E. coli*, the strain JLD271 harboring plasmids pSC11 and pJN105L was grown overnight. The overnight culture was diluted 1:10 in fresh LB medium supplemented with 100 $\mu\text{g}/\text{mL}$ ampicillin and 10 $\mu\text{g}/\text{mL}$ gentamicin. An appropriate amount of test compound stock solution (or OdDHL (**1**) stock solution for the positive control) in DMSO was added to clear 96-well microtiter plates (Costar 3370), with final DMSO concentrations not exceeding 1%. Once the subculture grew to an OD_{600} of ~ 0.25 , arabinose was added to a final concentration of 4 mg/mL to induce LasR expression from the plasmid pJN105L. The subculture was dispensed in 200- μL portions into each compound-treated well of the microtiter plate. Subculture containing 1% DMSO and no added OdDHL (**1**) was used as a negative control for minimal LasR activity. The plates were incubated with shaking for 4 h.

The cultures were assayed for β -galactosidase activity following the Miller assay method, optimized for microtiter plates (Griffith et al., 2002). The OD_{600} of each well was recorded, and 50- μL aliquots from each well were transferred to the wells of a solvent-resistant 96-well microtiter plate (Costar 3879) containing 200 μL Z-buffer, 8 μL CHCl_3 , and 4 μL 0.1% aqueous SDS. Cells were lysed by aspirating and dispensing the mixtures 30 times with a 12-channel micropipette, after which the CHCl_3 was allowed to settle for 5 minutes. A 100- μL aqueous aliquot from each well was transferred to a fresh clear-bottom 96-well microtiter plate. At $t = 0$ min, the assay was initiated by adding 20 μL of substrate, ortho-nitrophenyl- β -D-galactoside (ONPG; 4 mg/mL in phosphate buffer), to each well. This mixture was incubated at 30°C for 30 min, then 50- μL aliquots of a 1 M Na_2CO_3 solution was added to each well, terminating the reaction.

Absorbances at 420 and 550 nm were measured for each well using a plate reader. Miller units were calculated using the following formula: $1000 \times (A_{420} - (1.75 \times A_{550})) \times (\text{Time ONPG incubated with lysate in minutes})^{-1} \times (\text{Volume of culture lysed in mL})^{-1} \times \text{OD}_{600}^{-1}$. In all assays, Miller units were background-corrected relative to wells of LasR reporter subculture containing only 1% DMSO (no compound added). The OD-normalized Miller units of each compound was reported relative to the OD-normalized Miller units of a well containing enough OdDHL (**1**) to fully activate LasR.

All synthetic compounds were tested in technical triplicates, and ≥ 3 separate biological replicates were performed using unique cultures. EC₅₀ values, as well as respective 95% confidence intervals (CIs), were calculated using GraphPad Prism software (v. 6.0) using a sigmoidal curve fit. The dose-response curves are available in [Data S2](#).

Differential Scanning Fluorimetry Assay Protocol

The differential scanning fluorimetry (DSF) assay was performed according to previously published protocols using a LightCycler 480 instrument (Vivoli et al., 2014; Pantoliano et al., 2001). In brief, 20 μL samples were prepared containing individual LasR-LBD:**2**, **10–23** complexes (final concentration 0.25 mg/mL) and SYPRO Orange (5000x concentrate in DMSO; final concentration 5x). All samples were transferred into clear 96-well plates for thermal denaturation and fluorescence detection measurements. Thermal denaturation was achieved by heating up the plate from 25 to 95°C in a linear gradient over 1 h. The specific fluorescence was recorded, and the T_m for each complex was calculated. All experiments were performed in triplicate.

Purification and Crystallization of LasR-LBD:Compound Complexes

Each recombinant protein sample was purified from the above clarified supernatant using immobilized metal affinity chromatography (IMAC) charged with nickel sulfate. After elution, the His-tag was removed using PreScission Protease, and the protein was further purified by size exclusion chromatography (Superdex HiLoad 75 16/60, GE Healthcare) in 100 mM KCl, 20 mM HEPES (pH 7.5) buffer. The final concentration of purified protein was quantified by Bradford analysis (Thermo Scientific).

Each purified recombinant protein complex was subjected to crystallization using hanging drop vapor diffusion. In brief, 1 μL of protein solution (8–10 mg/mL) was mixed with 1 μL precipitant solution containing 80 mM calcium acetate, 40 mM HEPES (pH 7.3), 3 mM dithiothreitol, and 16% polyethylene glycol 4000. Crystallization trays were stored at 9°C, and crystals reached their maximum size after 2–7 days. Crystals of each complex were equilibrated with the precipitant solution supplemented with 30% of ethylene glycol, prior to vitrification by direct immersion in liquid nitrogen. Crystals suitable for X-ray diffraction were obtained with LasR-LBD:**10–17** and **19**.

Data Collection, Structure Determination, and Refinement

All diffraction data were collected on insertion device synchrotron beam lines (LS-CAT Sector 21 ID-F and ID-G, Advanced Photon Source, Argonne, IL). All data were indexed and scaled using either the HKL2000 or XDS package. Crystallographic phases were determined by the molecular replacement method as implemented in Phenix-Phaser using the coordinates of the previously solved 1.8 Å LasR-LBD structure without any water molecules or bound ligands (PDB Code = 2UV0). For each structure, iterative model building was carried out using Phenix-refine and further improved by manual fitting and adjustment using COOT. Crossvalidation, using 5% of the data for the calculation of the free R factor, was utilized throughout model building process in order to monitor building bias. The stereochemistry of all of the models was routinely monitored throughout the course of refinement using CCP4-PROCHECK. Relevant data collection and refinement parameters are listed in [Table S1](#), and stereo-views of electron density maps of the structures are shown in [Figure S1](#).

QUANTIFICATION AND STATISTICAL ANALYSIS

LasR agonism data were analyzed in GraphPad Prism (v. 6.0) using built in algorithms. EC₅₀ values were obtained in technical triplicates, and ≥ 3 separate biological replicates were performed using unique cultures. The values, as well as respective 95% confidence intervals (CIs), were calculated using a sigmoidal curve fit.

The Buried Surface Area (BSA, Å²) of each structure was calculated using the PDBePISA web tool (PDB in Europe-Proteins, Interfaces, Structures and Assemblies, http://www.ebi.ac.uk/msd-srv/prot_int/cgi-bin/piserver). In general, a monomer PDB file of each LasR structure (including the ligand coordinates) was uploaded to the web tool, and the BSA was calculated.

DATA AND SOFTWARE AVAILABILITY

Crystallographic coordinates for the protein structures reported in this paper have been deposited in and are freely available from the PDB (www.rcsb.org).